SAND2014-17243C

Suppressing Fine-Frequency Modes in Aluminum Nitride Microresonators

Darren W. Branch
Biosensors and Nanomaterials Department
Sandia National Laboratories
Albuquerque, NM USA
dwbranc@sandia.gov

Roy H. Olsson III
Advanced MEMS Department
Sandia National Laboratories
Albuquerque, NM USA

***Abstract*— Eliminating spurious modes in Aluminum Nitride (AlN) microresonators improves their insertion loss and quality factor by reducing acoustic energy leakage. Spurious modes that result from transverse wave propagation, termed fine-frequency modes, leak energy and propagate in the electrical busing and appear near the fundamental resonance. Although these modes can be predicted using three-dimensional (3D) finite element methods (FEM) for devices with very short acoustic length (e.g. 1 acoustic wavelength), 3D FEM is very slow and memory intensive when compared to a two-dimensional (2D) simulation. A fast 2D coupling-of-modes (COM) model was developed to predict, identify and implement strategies to suppress the fine-frequency modes.**

Keywords—Aluminum nitride, Spurious Modes, FEM, COM, Lamb Waves

I. INTRODUCTION

Aluminum Nitride (AlN) microresonators are known for their ability to realize multiple frequency filters on a single chip with frequencies ranging from 10 MHz to 10 GHz [1]. Their small size, high quality factor (Q), relaxed lithographic requirements, and temperature compensation using silicon dioxide, make them ideal for frequency control applications and integration with CMOS. The transduction mechanism is primarily based on the lowest-order symmetric Lamb wave (S0) propagating in a thinly supported membrane with an unloaded acoustic velocity in excess 10,000 m/s. Due to the width extensional (WE) excitation of Lamb waves using the d_{31} coupling and the free edges as broadband reflectors, a size reduction of 100x can be achieved compared to their surface acoustic wave (SAW) counterparts. Though the frequency and impedance of the width extensional mode is easily adjusted to accommodate a variety of different filter requirements, the presence of spurious modes degrades filter performance and limits applications [2-4].

Spurious modes are known to originate from several sources such as flexural wave propagation, acoustic interaction with the anchoring and busing and more recently mode conversion [4, 5]. In all these cases, the presence of spurious modes is dependent on the boundary conditions of the resonator at both the free-plate edges and the electrical busing terminations. Though the free-plates edges provide high reflectivity without increasing the size of the resonator, their broadband response does not suppress out-of-band spurious modes in contrast to Bragg reflectors. In some cases, mode conversion between the symmetric Lamb waves S0 and S1 at the plate edges has been observed to play a key role in spurious mode generation [5]. Mode conversion also can occur between the lowest-order (S0) symmetric Lamb wave and the anti-symmetric (A1) Lamb wave at specific wavelengths in temperature compensated AlN devices [4]. These large spurious modes can be suppressed by shifting the operating wavelength to avoid proximity of A1 and S0 modes. The smaller spurious or fine-frequency modes that appear near the fundamental resonance are from transverse wave propagation leaking energy into the busing, which will be referred to as spurious modes in this work.

Suppressing fine-frequency modes requires reducing energy leakage into the busing where it can propagate and causes small modes (~ 3 dB P-P) to appear near the fundamental resonance [6]. The fine-frequency modes are a function of the boundary conditions of the resonator at the electrical busing terminations. Several strategies have been investigated to suppress these modes such as using a narrow aperture to increase the separation of the transverse modes, apodization of the transducer or reflector [7], and using dummy fingers in the transducer [8]. Apodization is not desirable especially in AlN microresonators since it degrades the Q of the resonator and increases insertion loss. More recent suppression strategies aim to confine the acoustic energy by requiring that the acoustic velocity in the transducer region is smaller than the busing and external regions [9].

Simulation methods to study transverse mode propagation include scalar potential theory (SCP) [8, 10], two-dimensional (2D) coupling-of-modes (2D COM) [11-13], 2D P-matrix methods [14, 15] and the three-dimensional (3D) finite element method (3D FEM). SCP is a fast simulation method which is used to determine the length of stubs to suppress individually targeted transverse modes. It does not address 2D variation along the acoustic length or directly compute the electrical response. In contrast, the simulation time for the 3D FEM is still formidable since the thin electrode layer stacks used in AlN microresonators must be finely discretized. In some cases, effective material parameters approaches reduce the DOF but this still limits

Sandia is a multi-program laboratory operated by Sandia Corporation, a Lockheed Martin Company, for the United States Department of Energy under contract DE-AC04-94AL85000.

practical designs to a low number of electrode fingers, $N_t \cong 8$, with RAM requirements ~50-100 Gb due to meshing the thin films (Fig. 1). The 2D COM method is an intermediate model that can capture the physical effects of the electrical buss and transducer geometry without relying on 3D FEM. This work applies the 2D COM method across the entire structure. A separate 2D FEM model was used to calculate the COM parameters in the various domains for the 2D COM model.

II. Analysis

A. Theory

The 2D COM equations have previously been derived using the paraxial approximation which assumes the fields vary gradually along the axis of the independent variable [11, 13]. It is convenient to write the 2D COM equations in the partial differential equation (PDE) form as:

$$e_a \frac{\partial^2 u}{\partial t^2} + d_a \frac{\partial u}{\partial t} - \nabla \cdot \left(-c\nabla u + \alpha u - \gamma\right) + \beta \cdot \nabla u + au = f \qquad (1)$$

noting that the time dependent mass (e_a), damping (d_a), conservative flux (γ), and convection (β) terms are all zero. The 2D COM equations that involve the acoustic amplitudes can be written in form of (1) as:

$$\nabla \cdot \left(-c\nabla u\right) = \nabla \cdot j \begin{bmatrix} \begin{bmatrix} 0 & 0 \\ 0 & -\frac{\gamma_a}{2k_o} \end{bmatrix} & [0] \\ [0] & \begin{bmatrix} 0 & 0 \\ 0 & \frac{\gamma_a}{2k_o} \end{bmatrix} \end{bmatrix} \begin{bmatrix} 0 \\ \frac{\partial A^+}{\partial y} \\ 0 \\ \frac{\partial A^-}{\partial y} \end{bmatrix}$$

$$\nabla \cdot \left(-\alpha u\right) = \begin{bmatrix} 1 & 0 \\ 0 & 0 \\ 0 & 1 \\ 0 & 0 \end{bmatrix} \begin{bmatrix} \frac{\partial A^+}{\partial x} \\ \frac{\partial A^-}{\partial x} \end{bmatrix}$$

$$a = j \begin{bmatrix} -\delta & -\kappa_{12} \\ \kappa_{12}^* & \delta \end{bmatrix}$$

$$f = \begin{bmatrix} -\alpha V \\ \alpha^* V \end{bmatrix}$$

$$u = \begin{bmatrix} A^+ \\ A^- \end{bmatrix} \qquad (2)$$

$$\delta = k - k_o - j\gamma$$

where the A^+ and A^- are the forward and backward acoustic amplitudes, k_o is the wavenumber of the periodic structure, γ_a is the anisotropy parameter ($\gamma_a \cong 1$ for AlN), γ is the attenuation constant (Np/m), κ_{12} is the reflectivity, α is the transduction, V is the input voltage (V_i = 1), and δ is the detuning parameter or wavenumber deviation from the Bragg condition. The input (I_i) and output (I_o) currents are determined by integrating over the electrically active domains:

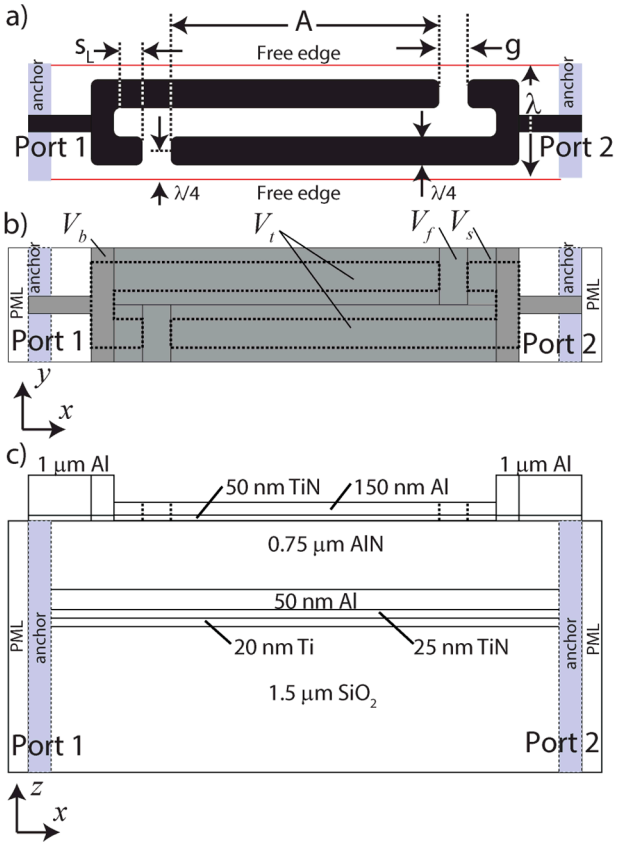

Fig. 1. Two-port AlN microresonator showing the input and output fingers connected to Port 1 and Port 2 for an $N_t = 2$ active fingers. a) The top metal (black) includes the transducer fingers and busing. The finger-to-stub gap (g) and stub length (s_L) are shown. The electrical ground is located underneath the entire structure. The period, p = λ/2. b) Equivalent field-model for the 2D COM simulation showing the domain and their respective velocity designations. The dotted region is the outline of the actual fingers, busing, and stubs in relation to the field-model. c) Cross-section of the AlN microresonator.

$$I_i(\omega) = \iint \left(2\alpha^* A^+ + 2\alpha A^- + j\omega C(x,y) V_i\right) dxdy$$
$$I_o(\omega) = \iint \left(2\alpha^* A^+ + 2\alpha A^-\right) dxdy \qquad (3)$$

where C is the static capacitance (F/m^2), and ω is the angular frequency. Though the static capacitance is spatially dependent, the variation is considered to be uniform across the transducer domain. The use of an electrically grounded bottom electrode underneath the entire structure requires integrating (3) in the transducer and busing domains. Continuity between the PDE domains for the acoustic amplitudes and their derivatives is achieved using Neumann boundary conditions [13]:

$$-n_1 \cdot \Gamma_1 - n_2 \cdot \Gamma_2 = -n_1 \begin{bmatrix} A^{\pm} \\ \pm j \frac{\gamma_a}{2k_o} \frac{\partial A^{\pm}}{\partial y} \end{bmatrix}_1 - n_2 \begin{bmatrix} A^{\pm} \\ \pm j \frac{\gamma_a}{2k_o} \frac{\partial A^{\pm}}{\partial y} \end{bmatrix}_2 = 0 \qquad (4)$$

Using the edges of the microresonator as broadband reflectors requires applying Dirichlet boundary conditions to obtain:

$$n\cdot\left(c\nabla u+\alpha u\right)+au=g-\mu$$
$$\mu=\begin{bmatrix}0\\0\end{bmatrix} \tag{5}$$

where reaction force (μ) on the boundary is zero. The expressions in (5) do not place any restrictions on the solution $A^{\pm}$ since μ is adjusted to satisfy the Dirichlet conditions. In the perfectly matched layer (PML) regions an absorbing boundary condition was used to damp incident waves by increasing the value of η to 1 along the length of the PML. The PML was defined by replacing the real wavenumber in the 2D COM equations with a complex form having a simple linear dependence:

$$k\left(r\right)\rightarrow k_f\left(1-j\eta\left(r\right)\right)=k_f\left(1-j\eta_o\frac{\left|r-r_i\right|}{d}\right) \tag{6}$$

where η_o is the attenuation in the PML region (η_o = 1), k_f is the wavenumber in the free domain, r_i is where the PML starts and r is the spatial coordinate, and d is the height of the PML, taken as 5·λ. To apply (2) to the domains in Fig. 1, the wavenumber k was redefined in terms of the velocity in each domain as:

$$\delta=k-k_o-j\gamma=\frac{2\pi\left(f-f_o\right)}{v}-j\gamma \tag{7}$$

where v is the velocity in each domain (Table I). The velocities in each domain were estimated by applying the 2D FEM to the material cross-section of each domain in the microresonator. The admittances were computed using the following:

$$Y_{11}=\left.\frac{I_i}{V_i}\right|_{V_o=0},Y_{21}=\left.\frac{I_o}{V_i}\right|_{V_o=0} \tag{8}$$

B. Microresonator

The structure of the microresonators consisted of a thin composite plate with input and output fingers alternating their connection from port 1 to port 2. For clarity, a device with N_t = 2 fingers is shown in Fig. 1, depicting the locations of the busing and fingers relative to the field model boundaries. Starting from the bottom of the AlN microresonators, the resonators were comprised of 1.5 µm of silicon dioxide (SiO_2), Ti/TiN/Al (20 nm/25 nm/50 nm) bottom electrode, and 0.75 µm of AlN. The top electrode layers consisted of TiN/Al (50 nm/100 nm) [2]. The free domains were un-metallized and the bottom electrode was electrically grounded. The domain and COM parameters are summarized in Table I. To simulate the device in Fig. 1, the COM parameters for the busing, free-space and stubs were substituted into (2). This model was implemented using the PDE mode of Comsol Multiphysics®. The 3D FEM was used to compare with measurements and the 2D COM approach.

TABLE I. DOMAIN PARAMETERS FOR 2D COM

λ = 16 µm		**2D COM Parameters**			
Domain	**δ**	**$\kappa_{12}p$**	**α ($\zeta p/\omega C_s$)**	**v (m/s)**	**C^a (pF/p/m)**
Transducer	k_t - k_o - $j\gamma$	-0.08	0.004	7873	512.3
Buss	k_m - k_o - $j\gamma$	0	0	7828	512.3
Free space	k_f - k_o - $j\gamma$	0	0	7910	0
Stub	k_s - k_o - $j\gamma$	-0.08	0.004	7873	512.3

[a] Additional shunt capacitance from the GSG pads was included using an external circuit.

III. RESULTS

Microresonators consisting of N_t = 2, 3, 4, 6, and 8 fingers were fabricated using the previously developed fabrication process. The two-port measurements shown in Fig. 2a, indicate that the fine-frequency modes were negligible in proximity to the fundamental resonance when $N_t \leq 4$, with several spurious modes located 30 dB down when N_t = 4. As N_t was increased the fine-frequency modes began to appear above the resonance frequency (Fig. 2b). This suggests that the acoustic length of the buss contributes to transverse mode propagation. Though the acoustic length of the buss can be reduced to suppress the transverse modes, this approach is not always practical due to the increased insertion loss. Instead direct suppression requires modifying the impedance of the boundaries between the buss and the transducer to eliminate all the fine-frequency modes while reducing the insertion loss.

A. 2D COM Analysis

Microresonators were simulated using 2D COM by converting them to an equivalent field model, where the acoustic ports were located λ/4 from the center of the fingers. The microresonators were divided into multiple domains in 2D, each with their own domain velocity: transducer (v_t), electrical busing (v_b), and free regions (v_f) (Fig. 1b). Previously, stubs were added to the busing to aid in suppression of the fine-frequency modes which were also included in this study [6]. Previous studies indicate that acoustic confinement occurs when the transducer velocity (v_t) is less than the velocity in the busing (v_b) [16] and free space (v_f): $v_t < v_b < v_f$, causing suppression of the fine-frequency modes. This because incident transverse waves arrive orthogonally to the electrical buss, complete reflection is achieved when $v_t < v_b$ since $\sin^{-1}(v_b/v_t)$ yields evanescent waves. Without any modification, the acoustic velocity in the electrical buss is almost always less than the velocity in the transducer ($v_b < v_t$). This condition causes acoustic energy to leak into the electrical buss and in turn propagate transverse modes (Table I). Fig. 3 confirms this finding, showing the presence of fine-frequency modes for the N_t = 8 device. In general the 2D COM model tracked well with the experimental measurements, where it was able to predict the first spurious modes located at -20 dB. However, the model exaggerated the amplitude of the spurious modes further

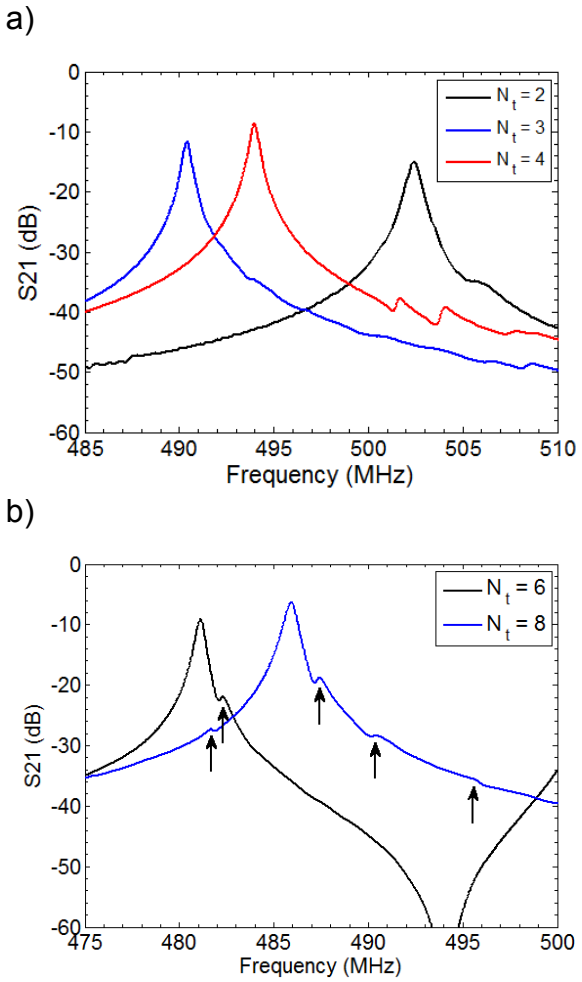

Fig. 2. S21 response a) AlN microresonators with N_t = 2, 3 and 4 fingers. b) When N_t > 4, fine-frequency modes (arrows) appear near the fundamental resonance. The N_t = 6 finger device also has a large anti-symmetric mode that was predicted using 3D FEM. λ = 16 µm.

away from the fundamental resonance, but preserves the shape of the spurious mode. This likely occurred for two reasons: the damping parameter (γ) in the 2D COM model was independent of frequency and the impact of the busing on the strain is not precisely captured especially further away from resonance. From the measurements, the second spurious mode was located at 490.3 MHz, where 2D COM predicted it at 491.3 MHz. In Fig. 3 the S21 data from the 2D COM simulation for the 2nd spurious mode had a similar but frequency shifted profile compared to the measurement and 3D FEM data. In the 2D COM simulations the quadrilateral mesh size was 1 µm, yielding a simulation time of 10 minutes using a 16-core processor machine under Linux RedHat®. The 3D FEM simulation predicted the first spurious mode at a slightly lower frequency than the measured data with smaller amplitude than measurement. However, the results of the 3D FEM were in good agreement with the spurious modes observed in the measurement. The simulation time for 3D FEM was 48 hours (5 minutes/ frequency point) using a tetragonal mesh with a DOF of 4.7 million under Linux RedHat®.

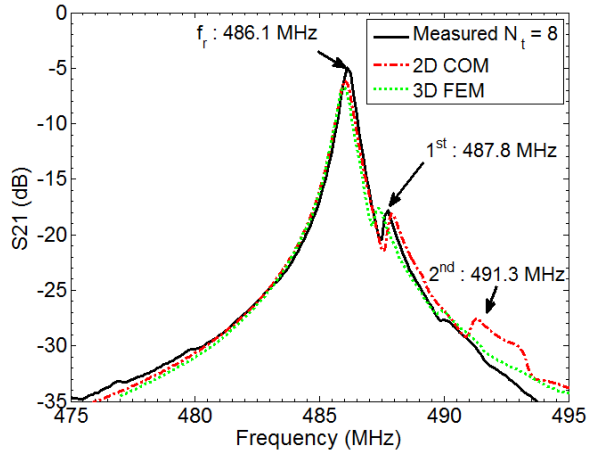

Fig. 3. Experimental and simulated S21 response with N_t = 8 fingers. The 2D COM simulation predicted two distinct spurious modes at 487.8 MHz and a second at 491.3 MHz. λ = 16 µm.

Using the 2D COM method, the acoustic amplitudes of transverse wave propagation were computed from the forward and backward propagating modes (Fig. 4). The two observable spurious modes are due to transverse wave propagation along the aperture. The fundamental resonance was symmetric along the aperture, where the two spurious modes appear as the 6th and 10th symmetric modes in the transverse direction. The field patterns demonstrate that the spurious modes leak more energy into the busing and free regions in Fig. 4b-c.

B. Suppression of Fine-Frequency Modes

To suppress the spurious modes the acoustic velocity in the transducer domain must be less than the velocity in the buss. To achieve this condition, a thin layer of silicon dioxide was added to the model (Fig. 5a). To simulate the addition of the silicon dioxide in 2D COM, the acoustic velocity in the transducer domain was gradually decreased. The admittances were computed for each transducer velocity to determine when the spurious modes were fully suppressed. Fig. 5 demonstrates the effectiveness of this

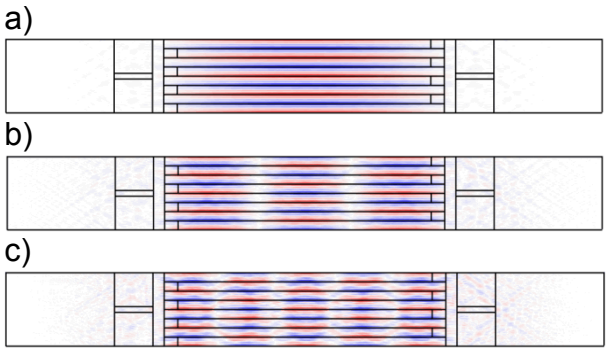

Fig. 4. Acoustic amplitudes from 2D COM simulation for N_t = 8 fingers. a) f_r = 486.1 MHz b) 1st spurious mode: f = 487.8 MHz, c) 2nd spurious mode: f = 490.1 MHz. The light regions are the nodes. The colored pattern is the Lamb wave. λ = 16 µm.

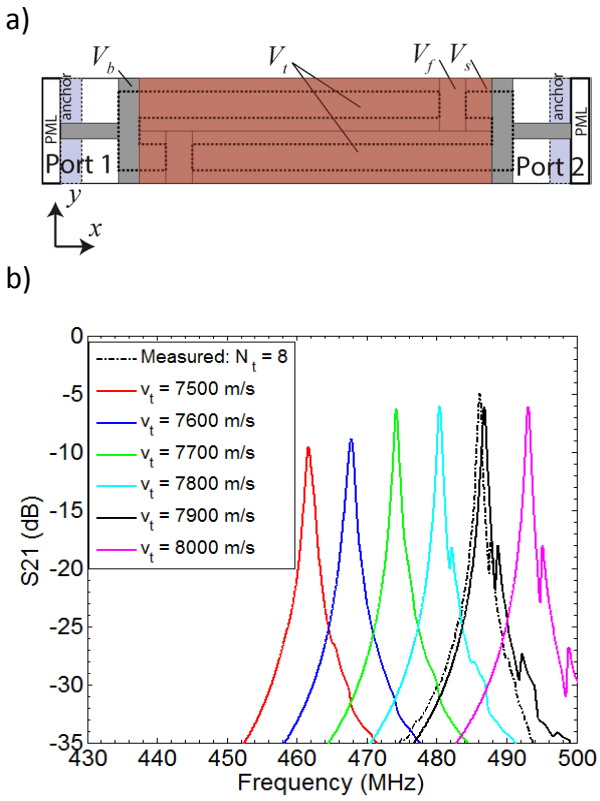

Fig. 5. Spurious mode suppression simulated using 2D COM. a) Silicon dioxide deposited in transducer region (red), b) Simulated S21 response with N_t = 8 fingers. Decreasing the acoustic velocity in the transducer domain suppresses spurious modes.

approach. By decreasing the acoustic velocity in the transducer to 7700 m/s both spurious modes were suppressed, corresponding to a silicon dioxide thickness of 0.7 µm. In contrast, artificially increasing the transducer velocity, achieved by reducing the finger thickness in the transducer domain, enhanced the spurious modes. In practice this would increase the motional resistance and degrade the Q. It is also critical that the free space velocity is higher than velocity in the buss and transducer: $v_t < v_b < v_f$.

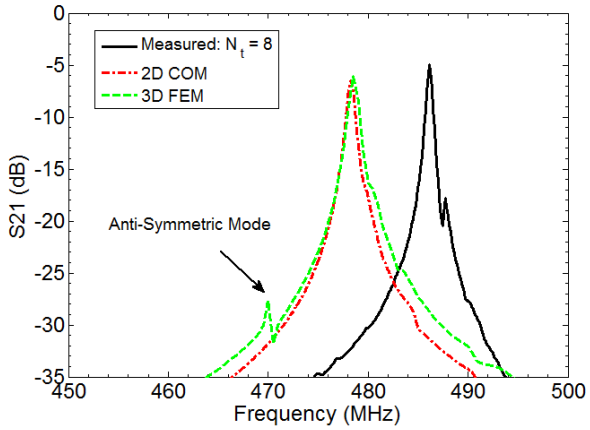

Fig. 6. Spurious mode suppression. The silicon dioxide layer was 0.7 µm thick on the transducer where the bottom temperature compensation layer was reduced to 0.8 µm.

When v_t < 7700 m/s, the spurious modes were fully suppressed with a noticeable decrease in S21, which is caused from an impedance mismatch. This suggests an optimal thickness exists to reduce acoustic loss while suppressing spurious modes. In Fig. 6, a 3D FEM simulation was performed to compare with the 2D COM simulation when 0.7 µm of silicon dioxide was deposited in the transducer region. To maintain temperature compensation, the bottom oxide layer was reduced from 1.5 µm to 0.8 µm. Because the top and bottom oxide layers alter the dispersion behavior of the microresonator, special care is required to suppress both anti-symmetric [4] and fine-frequency modes, while maintaining temperature compensation. In Fig. 6 a small anti-symmetric mode appears due to changing the bottom oxide thickness and the Q was slightly degraded. However, both fine-frequency modes were fully suppressed.

The 2D COM method is significantly faster than the 3D FEM, requiring 0.75 second/frequency point compared to 5 minutes/ frequency point for 3D FEM. The merits of the 2D COM method are the ability to sweep through larger parameter spaces to identify the locations of spurious modes and implement strategies for their suppression. Though narrow frequency sweeps using the 3D FEM method reduce computational time, the exact position of the resonance is not always known. This requires coarser sweeps that may under estimate the impact of smaller spurious modes appearing near the fundamental resonance.

IV. Conclusions

Transverse wave propagation along the acoustic aperture gives rise to fine-frequency modes that appear near the fundamental resonance. The source of these modes is attributed to transverse modes leaking acoustic energy which propagates in the busing. Since the acoustic velocity of the transducer is often lower due to the thicker metallized busing, additional dielectric layers such as silicon dioxide are suitable for decreasing the velocity in the transducer domain. The 2D COM method is an approximate technique to study the origin of fine-frequency modes and to investigate methods for their suppression. The addition of silicon dioxide eliminated the spurious modes where an optimal thickness is required to minimize acoustic loss.

Acknowledgment

Sandia National Laboratories is a multi-program laboratory managed and operated by Sandia Corporation, a wholly owned subsidiary of Lockheed Martin Corporation, for the United States Department of Energy's National Nuclear Security Administration under contract DE-AC04-94AL85000.

References

[1] G. Piazza, V. Felmetsger, P. Muralt, R. H. Olsson, and R. Ruby, "Piezoelectric aluminum nitride thin films for microelectromechanical systems," *MRS Bulletin,* vol. 37, pp. 1051-1061, Nov 2012.

[2] R. H. Olsson, J. G. Fleming, K. E. Wojciechowski, M. S. Baker, and M. R. Tuck, "Post-CMOS compatible aluminum nitride MEMS filters and resonant sensors," *Proceedings of the 2007 IEEE International Frequency Control Symposium Jointly with*

the 21st European Frequency and Time Forum, Vols 1-4, pp. 412-419, 2007.

[3] G. Piazza and A. P. Pisano, "Two-port stacked piezoelectric aluminum nitride contour-mode resonant MEMS," *Sensors and Actuators a-Physical,* vol. 136, pp. 638-645, May 16 2007.

[4] D. W. Branch, K. Wojciechowski, and R. H. Olsson, "Elucidating the origin of spurious modes in aluminum nitride microresonators using a 2-D finite-element model," *IEEE UFFC,* vol. 61, pp. 729-738, 2014.

[5] F. Thalamayr, K.-Y. Hashimoto, T. Omori, and M. Yamaguchi, "Fast Evaluation of Lamb Wave Scattering by Time Harmonic FEM simulation," in *Ultrasonics Symposium*, 2009, pp. 2805-2809.

[6] R. H. Olsson, K. E. Wojciechowski, and D. W. Branch, "Origins and mitigation of spurious modes in aluminum nitride microresonators," in *IEEE Intern. Ultrason. Symp. Proc.*, San Deigo, CA, 2010, pp. 1272-1276.

[7] W. H. Haydl, B. Dischler, and P. Hiesinger, "Multimode saw resonators - A method to study the optimum resonator design," *IEEE Ultrasonics Symposium,* pp. 287-296, 1976.

[8] Y. Yamamoto and S. Yoshimoto, "SAW transversely guided mode spurious elimination by optimization of conversion efficiency using W/W0 electrode structure," *1998 IEEE Ultrasonics Symposium - Proceedings,* vol. 1-2, pp. 229-234, 1998.

[9] H. Nakamura, H. Nakanishi, R. Goto, and K. Y. Hashimoto, "Suppression of Transverse-Mode Spurious Responses for SAW Resonators on SiO2/Al/LiNbO3 Structure by Selective Removal of SiO2," *IEEE Transactions on Ultrasonics Ferroelectrics and Frequency Control,* vol. 58, pp. 2188-2193, Oct 2011.

[10] R. V. Schmidt and L. A. Coldren, "Thin-Film Acoustic Surface Waveguides on Anisotropic Media," *IEEE Transactions on Sonics and Ultrasonics,* vol. Su22, pp. 115-122, 1975.

[11] H. A. Haus, "Modes in Saw Grating Resonators," *Journal of Applied Physics,* vol. 48, pp. 4955-4961, 1977.

[12] K. Hirota and K. Nakamura, "Analysis of SAW grating wavguides using 2D Coupling-of-Modes equations," *IEEE Ultrasonics Symposium,* pp. 115-120, 2001.

[13] O. Tokuda and K. Hirota, "Two-Dimensional Coupling-of-Modes Analysis in Surface Acoustic Wave Device Performed by COMSOL Multiphysics," *Japanese Journal of Applied Physics,* vol. 50, Jul 2011.

[14] G. Kovacs, "A generalised P-matrix model for SAW filters," *2003 IEEE Ultrasonics Symposium Proceedings, Vols 1 and 2,* pp. 707-710, 2003.

[15] K. Wagner, M. Mayer, A. Bergmann, and G. Riha, "A 2D P-Matrix Model for the Simulation of Waveguiding and Diffraction in SAW Components," *2006 IEEE Ultrasonics Symposium - Proceedings,* vol. 1-5, pp. 380-388, 2006.

[16] H. Nakamura, H. Nakanishi, R. Goto, and K. Hashimoto, "Suppression Mechanism of Transverse-Mode Spurious Responses in SAW Resonators on a SiO2/Al/LiNbO3 Structure," *2011 IEEE International Ultrasonics Symposium (Ius),* pp. 543-546, 2012.